International Journal of Mechanical Sciences 176 (2020) 105577

Contents lists available at ScienceDirect

International Journal of Mechanical Sciences

journal homepage: www.elsevier.com/locate/ijmecsci

A methodology for obtaining primary and secondary creep characteristics from indentation experiments, using a recess

M. Burley[a], J.E. Campbell[a], J. Dean[b], T.W. Clyne[a,*]

[a] Department of Materials Science & Metallurgy, Cambridge University, 27 Charles Babbage Road, Cambridge CB3 0FS, UK
[b] Plastometrex Ltd, Bradfield Centre, 184 Cambridge Science Park, Cambridge CB4 0GA, UK

ARTICLE INFO

Keywords:
Indentation
Inverse FEM
Creep
Recess

ABSTRACT

A procedure is described for Indentation Creep Plastometery (using a spherical indenter), which is analogous to that developed previously for Indentation Plastometry. As in that case, it is based on iterative numerical simulation of the indentation process, with repeated comparison between an experimental outcome and the corresponding model prediction, systematically varying the values of parameters in a constitutive law until optimal agreement is achieved. The constitutive law used here is the Miller–Norton relationship, which covers both primary and secondary creep regimes (although the transition between them is not well-defined). The experimental outcome is the penetration depth as a function of time, under a constant applied load. An important feature of the procedure is the prior creation of a spherical recess in the sample, having a pre-selected depth and a curvature radius equal to that of the indenter. This allows control over the stress levels created during the indentation creep testing and can be used to ensure that no (time-independent) plastic deformation is stimulated during the test. In the absence of such a recess, this is virtually unavoidable, since the stress levels created during initial contact between a spherical indenter and a flat surface tend to be very high. Such plasticity introduces unwanted complications into creep testing. Confirmation of the viability of the procedure is provided via comparisons between the creep characteristics of pure nickel samples at 750 °C, obtained in this way and via conventional uniaxial tensile testing.

1. Introduction

In view of the many advantages offered by indentation, compared with conventional uniaxial testing procedures, the development of methodologies that allow the extraction of reliable plasticity characteristics from indentation data is an important goal. Much of the work carried out so far has been focused on (quasi–static) plasticity (yield stress and work hardening parameters). However, there is also considerable interest in creep. A number of analytical or semi-analytical procedures [1–9] have been developed for obtaining creep characteristics from instrumented indentation data. Most commonly, the aim is to evaluate the stress exponent, n, that applies during the secondary creep regime. These procedures inevitably involve gross simplification of the complex stress and strain fields created as an (elastic) indenter penetrates into a sample via creep deformation. In general, the outcomes (such as inferred n values) from such analytical procedures are very unreliable, for reasons that have become clear [10–13]. One of the complications is that the primary regime of creep tends to influence the overall outcome throughout the test (because the creep strain field is continually expanding).

Iterative FEM simulation of the indentation process, on the other hand, offers the potential for accurate capture of evolving stress and strain fields, particularly if a constitutive law is used that covers both primary and secondary creep behavior. In fact, the iterative FEM methodology is now quite well developed and reliable [14–21] for extraction of plasticity characteristics from indentation data (either load-displacement or residual indent profile) and software packages are becoming available that allow automated extraction of such properties.

The current paper is focused on Indentation Creep Plastometery, for which the state of development is less well advanced. The procedure commonly involves the application of a constant load to a sample via a (spherical) indenter. The load is held at this level for an extended period, during which progressive penetration of the indenter into the sample is monitored. As with Indentation Plastometry, iterative FEM modeling of the process is carried out, with the creep characteristics (primary and secondary) captured in a constitutive law. Furthermore, the technique has the attraction of effectively investigating the creep response of the material over a range of stress levels during a single test (whereas separate tests are needed for different stress levels during conventional testing). Also, the FEM simulation is based on true stress levels, whereas a drawback of conventional creep testing is that, unless

* Corresponding author.
E-mail address: twc10@cam.ac.uk (T.W. Clyne).

https://doi.org/10.1016/j.ijmecsci.2020.105577
Received 7 October 2019; Received in revised form 26 February 2020; Accepted 3 March 2020
Available online 4 March 2020

the applied load is varied during the test (using a feedback loop based on the measured length change), the true stress changes progressively during the test as the specimen sectional area changes.

In view of these attractions, there is every prospect of Indentation Creep Plastometery becoming widely used in due course. While the level of activity and development has been lower than those for indentation plastometery, a number of relevant papers [22–28] have been published. There are also patents [29,30] concerning the extraction of creep parameters via some kind of local deformation of a sample. In fact, one of the main stumbling blocks so far has been the difficulty of carrying out an indentation creep test without stimulating (quasi-static) plasticity in the sample at the same time, particularly during the early stages of the test. A simple procedure is described here that circumvents this problem.

2. Experimental procedures

2.1. Introduction of a recess prior to indentation creep plastometry

The procedure, as previously employed, incorporates a major difficulty. It is important, when carrying out creep testing, to avoid (time-independent) plastic deformation. During conventional (uniaxial) creep testing, this is easily achieved by ensuring that the applied stress level is below the yield stress (for the temperature concerned). During indentation creep testing, however, the induced stress levels tend to be very high initially (when the contact area between the indenting sphere and the flat surface of the sample is small). Some plasticity is difficult to avoid during this phase, even if attempts are made to ramp up the applied load in some controlled way. This is doubly unfortunate, since (a) the displacement due to plasticity is difficult to separate from that due to creep during this initial period and (b) inducing plastic deformation may change the microstructure in such a way as to affect the creep response.

During the current work, a spherical recess was introduced in the sample before the start of the test, with a depth equal to half of the indenter radius - ie $\delta_0 = 1$ mm, with an indenter radius of 2 mm. For any selected recess depth, use of the FEM model allows the stress field in the sample to be predicted, making it easy to ensure that the maximum (deviatoric) stress does not exceed the yield stress (for the temperature concerned). In the present case, the value of 1 mm was found to be sufficiently deep to ensure that this condition was met, for the largest load that was used. Making it deeper than this would, of course, have reduced these stresses further, but this would have had the disadvantage of reducing the depth range over which the creep experiments could be carried out: if the “immersion depth” of the sphere were to approach its “equator”, then the boundary conditions would change and the modeling become more problematic. This development is the subject of a recently-filed patent [31].

2.2. Physical creation and characterization of the recess

The shape of the recess should match that of the indenter. It may in practice not be important for the matching to be very good (since local irregularities are likely to be quickly removed once the creep testing has started), but in the present work an attempt was made to obtain excellent matching. It may also be noted at this point that a typical indenter radius is expected to be of the order of 1–2 mm. Since this is relatively coarse (ensuring that a representative volume of the sample is being mechanically interrogated), the scale of the recess is such that conventional machining procedures can be employed to create it. On the other hand, the region being tested is still relatively small, so the sample can be small and the mapping of properties over a relatively large sample is still possible.

A recess of approximately the desired shape and depth was first created using a conventional drill bit with a spherical tip. A smooth recess surface, closely matching that of the indenter, was then created using a drill with an indenter as the tip. By introducing abrasive powder into the recess, this essentially becomes a honing operation that will create a smooth recess with a topography closely matching that of the indenter. Furthermore, by using a profilometer (optical or contact), the actual shape of the indent can be accurately captured and this can be used both to check on whether the surface finish and overall topography are acceptable and also to create the FEM mesh that will be used during iterative simulation of the indentation test. Since the depth of the recess is likely to be of the order of at least several hundred microns, the resolution requirements of the profilometry are relatively undemanding - a value of the order of 1 μm is typically sufficient.

2.3. Securing of the indenter and double sample operation

A potentially important issue, particularly when testing highly creep-resistant materials, concerns the possibility of inelastic deformation occurring within the housing of the indentation sphere during the test. This housing is most conveniently made of metal, but this leads to the possibility of creep occurring within it close to the indenter, in a similar way to that occurring in the sample. This would introduce errors in the measured displacement-time data. This was eliminated in the current work by using two identical samples, both with recesses, located above and below a free-standing (ceramic) sphere. Not only does this eliminate the possibility of errors arising from an unknown contribution to the displacement from deformation within the housing, but also the magnitude of the measured displacement is doubled, thus improving the accuracy of the data.

2.4. Sample preparation

The results reported here relate to samples of pure nickel, obtained from Goodfellows in the form of extruded cylindrical rods of 10 mm diameter. An optical micrograph is shown in Fig. 1, where it can be seen that the grain size was around 50–100 μm and the grain structure was approximately equiaxed. The temperature of all tests was fixed at 750°C. It was confirmed that the degree of oxidation of these samples, at this temperature, was negligible.

2.5. Uniaxial tensile stress–strain testing

For uniaxial tensile stress-strain testing, samples were in the form of cylindrical dog-bone samples, with a gauge section diameter of 3.1 mm and a length of 22 mm. Samples were gripped using collets made of CMSX-4. Strain was measured using an MTS 632.54F-14 axial extensometer (clip gauge), with a gauge length of 12 mm. Tensile stress-strain curves at 750°C were obtained using an Instron LCF testing machine. A typical outcome is shown in Fig. 2, which presents the data as both nominal stress against nominal (plastic) strain and true stress against

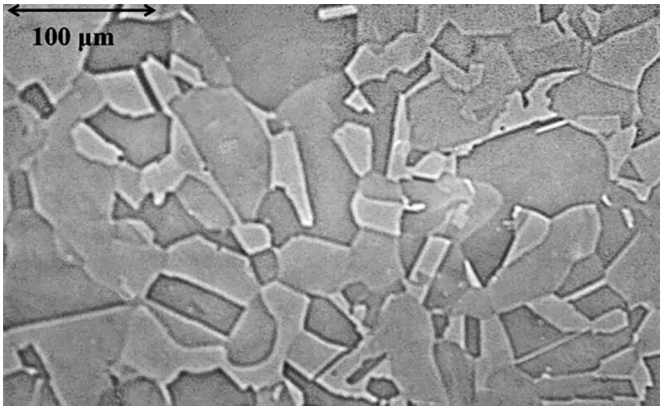

Fig. 1. Optical micrograph of the Ni.

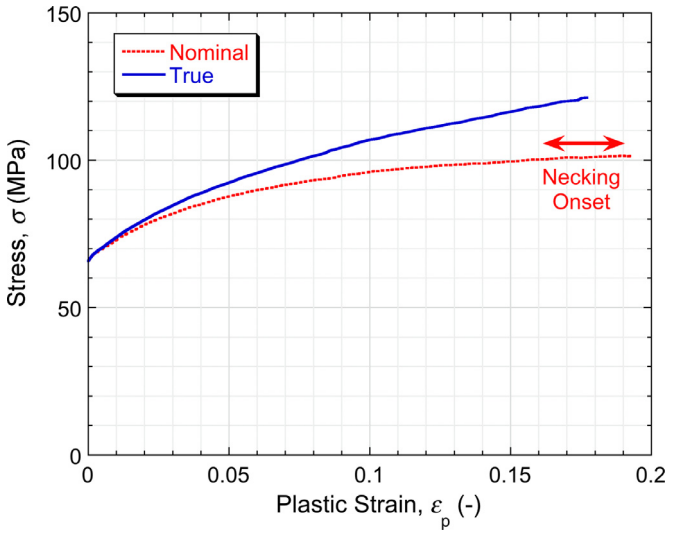

Fig. 2. Tensile stress-strain curves for the Ni at 750 °C, plotted as both nominal stress v. nominal strain and true stress v. true strain (obtained via the analytical relationships, assuming that the stress and strain fields remained uniform throughout).

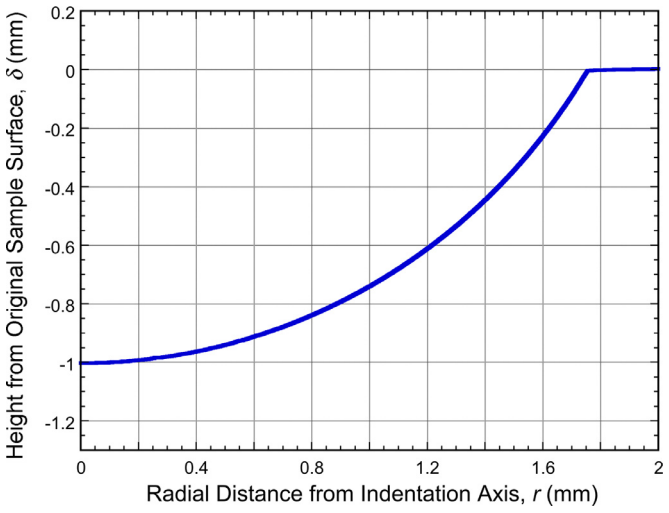

Fig. 3. Profile across a recess, measured using a contact stylus.

true plastic strain. It can be seen that the yield stress is about 66 MPa, with some subsequent work hardening.

2.6. Uniaxial tensile creep testing

Uniaxial tensile creep testing was carried out using the same machine, sample dimensions and set-up as for the stress–strain testing. The (nominal) stress levels employed were 35, 45 and 55 MPa. These levels were chosen to ensure that they were below the measured yield stress, so that conventional plasticity did not occur. The target duration for these tests was 5 10^4 s (~14 h), although the 55 MPa test was stopped before that, since the strain rate had become high and it seemed likely that necking and/or rupture was imminent.

2.7. Indentation creep testing

The indenter used was a sphere of 4 mm diameter, made of Si_3N_4 (supplier Bearing Warehouse Ltd). The recess in the sample had a depth of 1.0 mm. It was produced by first using a spherical end drill of diameter 4 mm and then using an identical sphere to that used in the creep testing, attached to the end of a drill bit. SiC polishing powder (~1 μm) was inserted into the recess before this honing operation. This ensured that the shape of the recess closely matched that of the indenter. A Taylor Hobson (Talysurf) profilometer (ie a contacting stylus), with a wide-range inductive gauge and 20 μm radius cone recess tip, was used to measure the recess profile (assumed to be radially symmetric). The height resolution of these scans is about 1 μm. Tilt correction functions were applied to the raw data, based on the far-field parts of the scan being parallel. A scan to the axis of the recess is shown in Fig. 3.

The indentation creep tests were also carried out over a period of 5 10^4 s. Constant loads of 0.85 and 1.0 kN were used. FEM simulation was used to ensure that, with this configuration, and with these loads, the peak (von Mises) stress created under the indenter was below the uniaxial yield stress. The creep indentation experiments were carried out using double sample set-ups of the type described in §2.3. The samples were cylinders of diameter 10 mm and thickness 10 mm. An FEM mesh is shown in Fig. 4 and the von Mises stress field created when a load of 1 kN is first applied is shown in Fig. 5. It can be seen that the stress levels in the sample do not reach the yield stress. The peak value is about 50 MPa. It may be noted that, during this type of test, the stress levels will tend to fall as the indenter penetrates more deeply into the sample - see below. (This is not necessarily the case during conventional plastic deformation, when work hardening can cause stress levels below an indenter to rise as it penetrates more deeply.)

3. FEM model formulation issues

3.1. Constitutive law

In addition to checking that conventional plastic deformation would not occur during indentation tests, FEM simulation of the process was used to predict the outcome of the test (penetration–time plot), for given combinations of applied load and the set of parameter values in the constitutive law used to represent the creep behavior. The expression used in the current work was the Miller-Norton law, which may be written:

$$\varepsilon_{cr} = \frac{A\sigma^n t^{m+1}}{m+1} \exp\left(\frac{-Q}{RT}\right) \tag{1}$$

in which A is a constant (units of MPa^{-n} $s^{-(m+1)}$), t is the time (s), n is the stress exponent and m is a dimensionless constant. This law is designed to capture both primary and secondary regimes of creep (and the transition between them). This is essential [10] for indentation creep work, in which a steady state (purely secondary creep) is never established. Since only a single temperature was used in the current work, the exponential term was also constant and the symbol C is now used to represent the product of this term and A.

It should be noted how this equation was employed in order to obtain the increments of strain generated in a given volume element as it experiences a changing (deviatoric) stress throughout the test. The equation can be differentiated with respect to time, to give

$$\dot{\varepsilon}_{cr} = C\sigma^n t^m \tag{2}$$

The time can thus be expressed in terms of both strain rate and strain:

$$t = \left[\frac{\dot{\varepsilon}_{cr}}{C\sigma^n}\right]^{1/m} = \left[\frac{(1+m)\varepsilon_{cr}}{C\sigma^n}\right]^{1/(1+m)} \tag{3}$$

Eliminating t and rearranging allows the strain rate to be expressed as a function of the strain:

$$\dot{\varepsilon}_{cr} = \{C\sigma^n\}^{1/(1+m)}\left[(1+m)\varepsilon_{cr}\right]^{m/(1+m)} \tag{4}$$

It is assumed that the cumulative creep strain defines the 'state' of (a volume element of) the material, with the instantaneous creep strain rate determined by the current stress (in the volume element concerned) and the prior strain: the creep strain rate can thus be expressed solely as a function of the creep strain. This is depicted in Fig. 6 and details

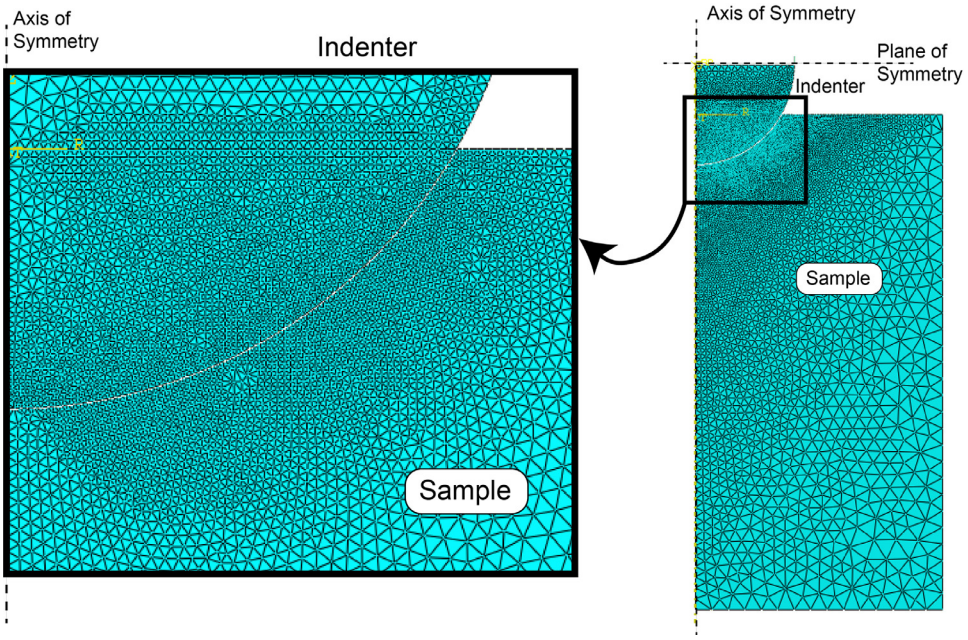

Fig. 4. Initial FEM Mesh for simulation of indentation, using a recess and a double sample.

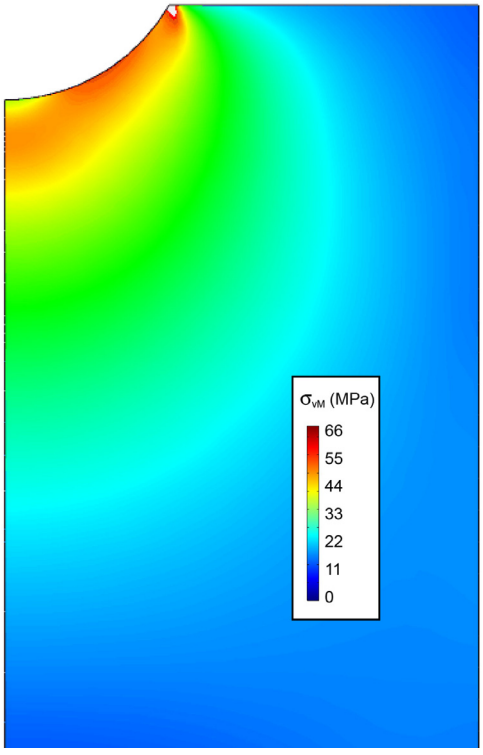

Fig. 5. Predicted von Mises stress field within the sample on application of a load of 1 kN to an indenter of radius 2 mm, with a prior spherical recess created in the sample, having the same radius as the indenter and a depth of 1 mm.

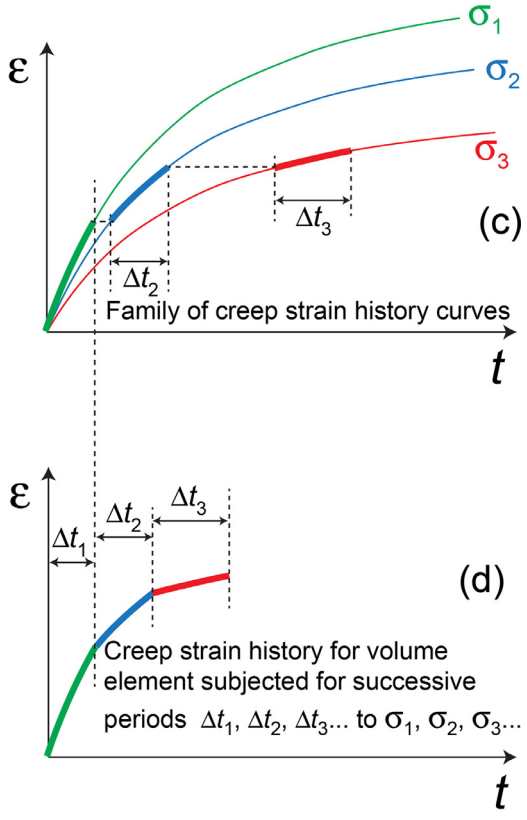

Fig. 6. Schematic illustration of how the creep strain history of a volume element is assumed to be composed of a series of incremental strains, each dependent on the creep curve for the stress level concerned and the prior cumulative creep strain experienced by the element.

of the algorithm are supplied elsewhere [25]. In summary, during each time increment, the net displacement of the indenter is found (within Abaqus) by monitoring the cumulative creep strain in each element up to that point, taking account of the (von Mises) stress in it, using Eq. (4) to obtain the further strain that will arise in it during the time interval and then using compatibility conditions to solve and give the overall shape change of the domain.

The procedure for obtaining the "best-fit" set of values for C, n and m involves systematic migration in parameter space until convergence is obtained, using a "goodness-of-fit" parameter to characterize the level of agreement between measured and predicted test outcomes (penetration-time plots). This is described below.

A friction coefficient must be specified for the FEM modeling. For most of the work described here, the value used was 0.2. A brief examination of the sensitivity of the outcome to the value of μ is described in §4.2.

3.2. Model meshing and boundary conditions

The current work involved FEM simulation of (spherical) creep indentation, with prior production of a recess. Both the radial and axial extent of the domain, relative to the indenter radius, need to be large enough to ensure that they do not affect the outcome. (This also needs to be true for the experimental set-up.) It was confirmed that this was the case for the domain shown in Fig. 4, and for the actual samples. For this case (ie effectively semi-infinite samples), there is no need to match the mesh to the actual dimensions of the sample and the FEM modeling outcomes will be applicable to any sample dimensions that satisfy this condition.

3.3. Convergence algorithm

The algorithm used to converge in parameter space on the best fit combination of parameter values is the Nelder–Mead simplex search [32]. This was chosen in view of its robustness and adaptability, particularly with respect to noise. The procedure used is based on that of Gao and Han [33], and was built using the Scientific Python and Numeric Python packages [34,35]. Full details are available elsewhere [18].

The goodness-of-fit between target and modelled data (displacement-time data) is characterized here via a dimensionless parameter S_{red}, a "reduced sum of squares of the residuals".

$$S_{\text{red}} = \frac{\sum_{i=1}^{N} \left(\delta_{i,\text{M}} - \delta_{i,\text{E}}\right)^2}{N \delta_{N,\text{E}}^2} \tag{5}$$

where $\delta_{i,\text{M}}$ and $\delta_{i,\text{M}}$ are respectively the modelled and experimental values of the displacement, at times varying from 0 up to t_{max} (split into increments of Δt and with the counter i varying from 1 to N). The actual number of measured values would commonly run into thousands, but a typical value of N would be of the order of 100, so some filtering and averaging of the raw data was employed. The normalising displacement, $\delta_{N,\text{E}}$, is the experimental value at the end of the run ($i = N$).

This operation could be carried out for just a single run - ie for a single value of the applied load, P. However, in the current work, two runs (with different values of P) were carried out, so two $\delta_{i,\text{E}}$ datasets were available. For each combination of M-N parameter values (giving a $\delta_{i,\text{M}}$ dataset for each P), the S_{red} value was calculated in each case and the numerical average taken. In this way, equal weighting was given to the two runs. Of course, more runs could be included in this operation, although it is important to note that even a single run creates a wide range of (changing) stress levels within the sample, up to a level predetermined by the load P and the penetration ratio of the recess ($\delta_{0,\text{E}} / R$, where R is the indenter radius). Among the several compromises involved in choice of the conditions is that of having this ratio large enough to ensure that the peak stress (for the P concerned) does exceed the yield stress, while leaving a large enough range of $\delta_{i,\text{E}}$ (up to $\delta_{\text{i,E}} = R$ - ie reaching the "equator", which is probably as deep a penetration as would normally be envisaged).

As for the corresponding parameter for plasticity [21], S_{red} is thus a positive dimensionless number, with a value that ranges upwards from 0 (corresponding to perfect fit). Modeling that captures the material creep response well should lead to a solution (set of parameter values) for which S_{red} is relatively low - say, less than 10^{-3}. This effectively constitutes a health check on the solution - if, for example, no solution can be found giving a value smaller than, say, 1%, then this suggests that there can only be limited confidence in the inferred set of values. This could be due to experimental deficiencies and/or an inability to capture the behavior well with the constitutive law being used. In fact, during the work described here, a solution with an S_{red} value well below 10^{-3} was found, representing very good agreement.

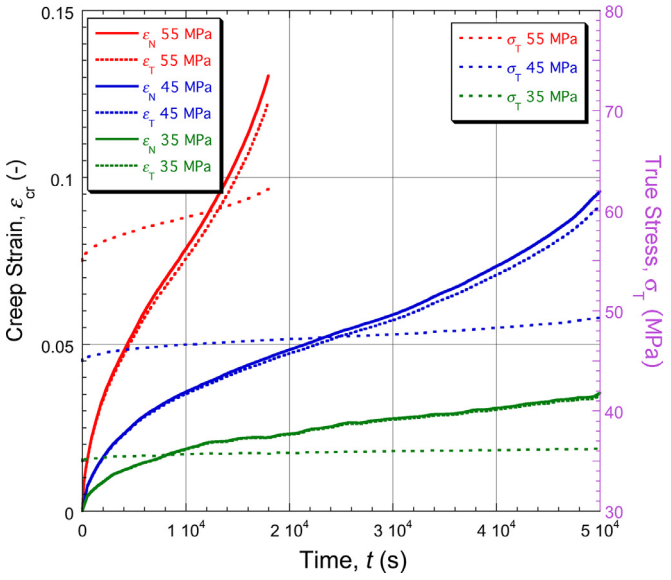

Fig. 7. Experimental data from tensile creep testing with three different (nominal) stress levels. Both nominal and true creep strains are plotted. Also shown are the changing values of the true stress during each of these tests.

4. Test outcomes

4.1. Uniaxial tensile creep results

The outcomes of tensile creep testing with the 3 different levels of applied (nominal) stress are shown in Fig. 7. It can be seen that these all exhibited shapes broadly expected of creep strain curves, with those for the higher stress levels showing what appear to be "tertiary" regimes of increasing strain rate towards the end of the test - ie at strains of the order of 10%. There is also a clear "primary" regime in all cases, which for these tests constituted a significant proportion of the test (in terms of both strain and time). In fact, at least for the two higher stress levels, there is not really any well-defined "secondary" regime of constant strain rate. This is actually quite representative of much creep testing, at least with relatively high stress levels.

It may be noted at this point that, at least for the 55 MPa test, the true stress level started to exceed 60 MPa, and thus became quite close to the measured yield stress (of about 66 MPa) in the "tertiary" regime. For the 45 MPa test, on the other hand, the true stress was still below 50 MPa at the time when the strain rate started to rise.

4.2. Indentation creep results

The experimental indentation (displacement-time) data for the two loads employed are shown in Fig. 8, together with corresponding predictions for the (best fit) set of Miller–Norton parameter values shown. Also shown are the final S_{red} values obtained in each case. Convergence on these best fit values is illustrated by the plots shown in Fig. 9, in which the misfit parameter value is the average of those for the two loads. It can be seen that convergence was achieved within about 60–80 iterations. This is broadly typical, although it does depend on the starting point in parameter space. A fairly random starting point (which can be seen by inspection of Fig.9(b)–(d)), was used in this work. If there were some prior information available about the likely values of the parameters, then a starting point could be chosen that was closer to the "correct" answer, in which case convergence would be quicker.

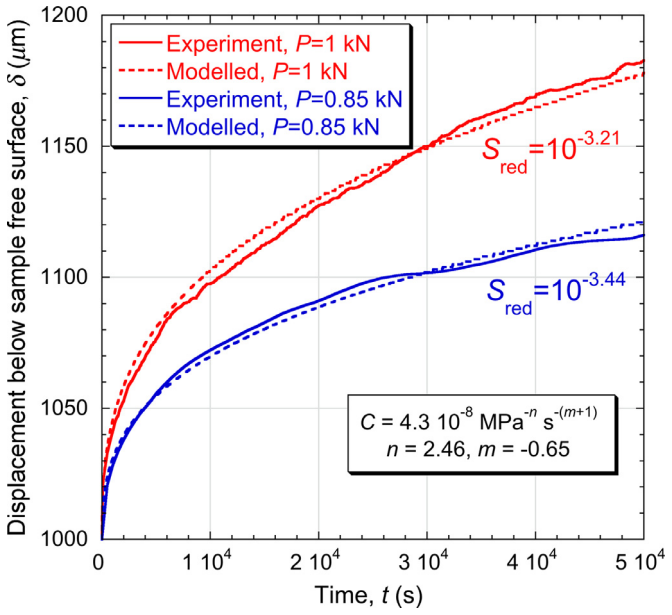

Fig. 8. Comparison between measured and (best-fit) modeled penetration histories during indentation with two different applied loads. Also shown are the best fit Miller–Norton parameter values and the final values of the misfit parameter in each case.

The real time required to reach a solution was fairly short, although of course this will depend on the computational power available.

Information about the sensitivity of the outcome to the value chosen for the coefficient of friction is provided by the curves in Fig. 10. A lower value gives more frictional sliding, allowing the indenter to penetrate more deeply. The fact that differences are observed over the complete range of μ used in the plot indicates that none of the values are high enough to completely eliminate sliding or low enough to ensure that it is uninhibited. However, the sensitivity is relatively low and a value of 0.2 is considered representative. It might be feasible in future work to include the value of μ in the set of parameters to be optimized, since it is not really possible to measure it directly in any other way.

4.3. Tensile creep curves from indentation outcomes

The main objective is to obtain conventional (tensile) creep data (for any selected level of applied stress), at least in primary and secondary regimes, solely from indentation experiments - in fact, essentially from a single indentation experiment. All that is required is the best fit set of Miller–Norton parameter values. These can then be used to predict the outcome of creep testing with any configuration, including, of course, the simple one of uniaxial tensile testing. In fact, for that case, it's not even necessary to carry out any further FEM modeling, since a tensile creep test is one in which the stress and strain field tends to remain homogeneous. (This is not true for compressive creep, when friction and barreling tend be significant.) A comparison between the outcome of a tensile creep experiment and a prediction based on indentation-

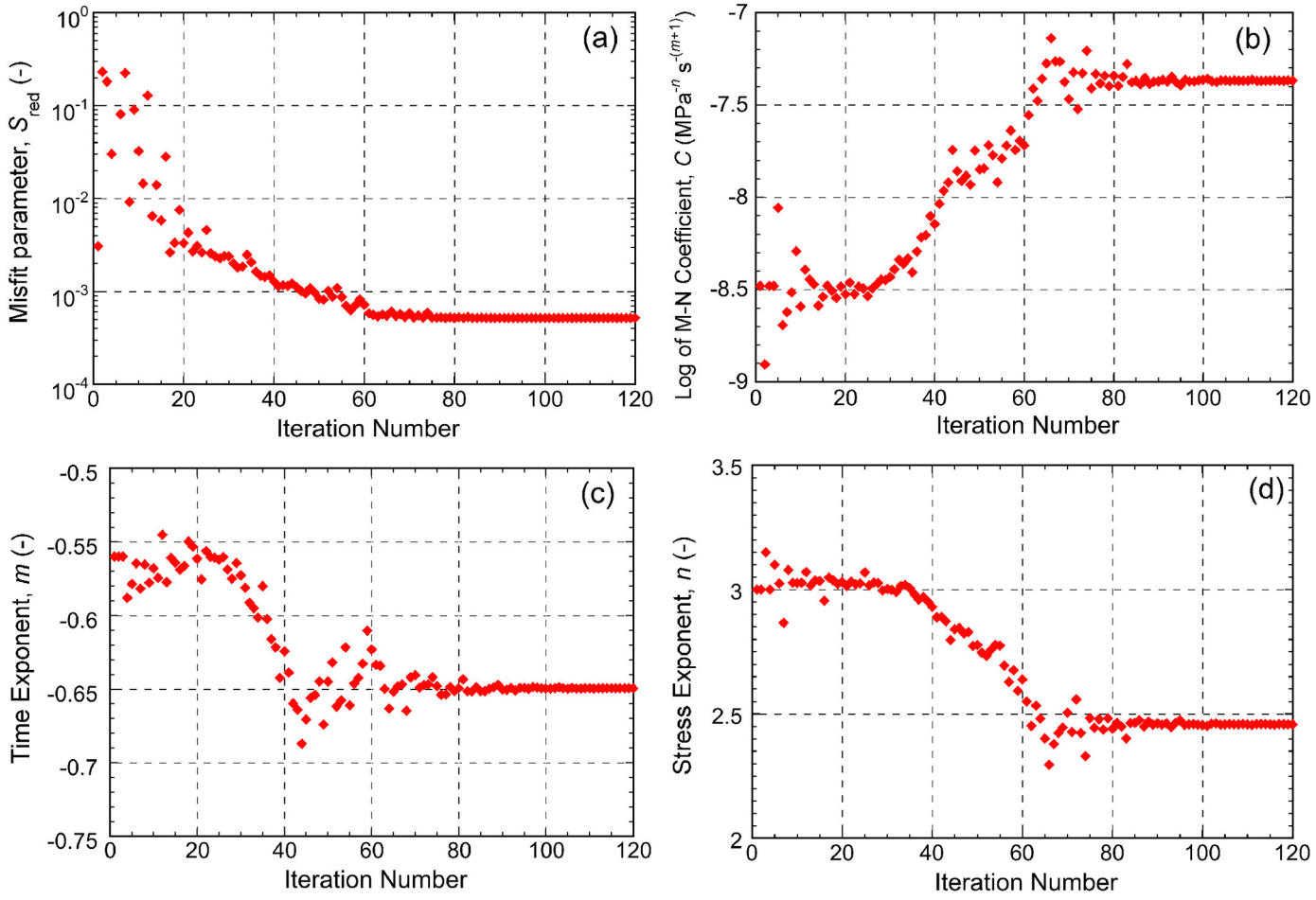

Fig. 9. Nelder–Mead convergence on an optimal Miller–Norton parameter set, targetting the two displacement–time plots during indentation, showing the evolution with iteration number of: (a) the goodness-of-fit parameter, S_{red}, (b) the M-N coefficient, C, (c) the time exponent, m and (d) the stress exponent, n.

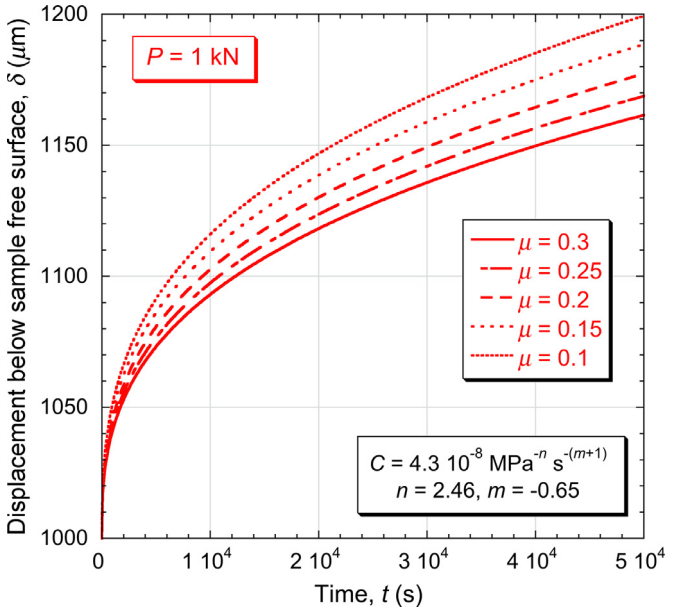

Fig. 10. Modeled penetration histories during indentation with an applied load of 1 kN, for several different values of the coefficient of friction.

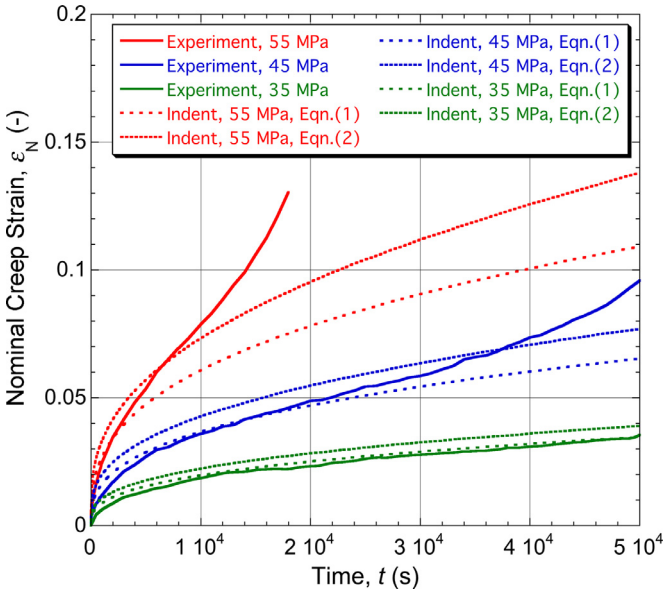

Fig. 11. Comparison between creep strain curves obtained by conventional tensile testing, with a fixed nominal stress, and those obtained via iterative FEM modeling of indentation creep with a constant applied load, using the Miller–Norton expression in one of two forms.

derived values of the Miller–Norton parameters can therefore be made via simple manipulation of the Miller-Norton equation.

The outcome of such an operation can be seen in Fig. 11, where the experimental plots of the nominal creep strain as a function of time (from Fig. 7) are compared with corresponding predicted plots obtained using the indentation-derived Miller–Norton parameter values. Two sets of these are shown. The first is simply the curve corresponding to Eq. (1), with the true creep strain obtained in that way converted to a nominal strain and the stress used in the equation being fixed at the nominal value. The second is based on the strain rate form of the M-N expression – ie Eq.(2). This has been implemented by stepping through a series of time increments, calculating the latest strain rate by taking into account the changing value of the true stress. This is how the Miller–Norton expression should be used, since both the stress and the strain in it are true values. It can be seen that doing this makes a significant difference to the predicted curves, although in these cases it does not lead to any increase in the overall strain rate with increasing time. (This would tend to happen at higher strains, depending on the value of n.)

The most striking feature of Fig. 11 is that the agreement between conventional tensile creep testing and the indentation-derived outcome is in general very good, at least within the primary and secondary regimes. The "tertiary" regime, which is quite noticeable with the highest level of applied stress, is not captured, even by using the Miller–Norton formulation in a way that takes account of the increasing level of true stress in such tests. It is possible that this discrepancy is due to the true stress starting to approach the yield stress at the temperature concerned. If this happens, then it is expected that the behavior will not be captured well using a creep model of this type, and plasticity characteristics (including the work hardening rate) are likely to have an effect. In fact, any analytical formulation, such as the Miller-Norton law, is likely to be reliable only within a certain range of (true) stress.

It is of interest to note the range of stress and strain generated within an indentation test of this type, since it is clear that creep characteristics well outside of these ranges are unlikely to be captured well by such a test. Fig. 12 shows fields of (von Mises) stress and creep strain within the sample at the end of the simulation with an applied nominal stress of 55 MPa. (This is actually after a time of 5 10^4 s, whereas the corresponding tensile creep test was stopped after about 1.8 10^4 s, when the strain rate was becoming very high.) This case therefore reflects a relatively severe test, in terms of generating high stresses and strains. It can immediately be seen, on comparing Fig. 12(a) with Fig. 5, that the stress levels have relaxed somewhat as the indenter has penetrated, and all of these stresses are well below the yield stress. It can also be seen from Fig. 12(b) that the creep strains generated within the sample range up to about 10–15%, which is appropriate for the comparisons shown in Fig. 11.

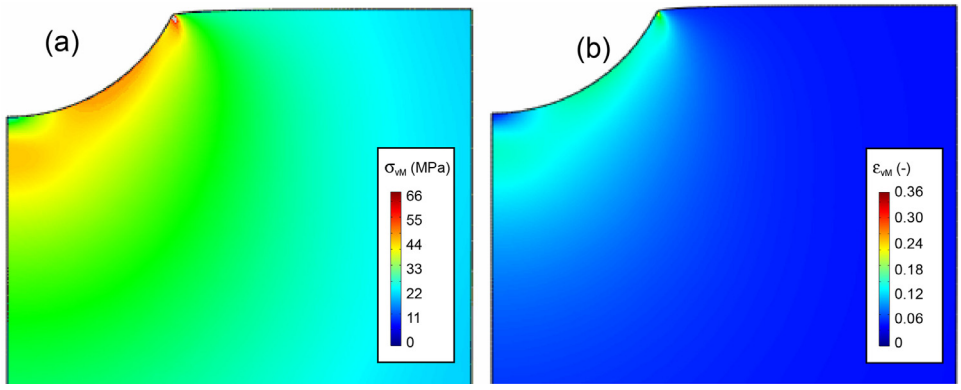

Fig. 12. Predicted von Mises (a) stress and (b) strain fields within the sample 5 10^4 s after application of a load of 1 kN to an indenter of radius 2 mm, with a prior spherical recess created in the sample, having the same radius as the indenter and a depth of 1 mm.

Finally, it can be see in Fig. 12 that there is some "pile-up" around the indent, although it is not very pronounced. Of course, during conventional plastic deformation, such pile-ups can be quite noticeable, particularly for materials that exhibit little work hardening (allowing large plastic strains to develop near the pile-up). In general, while there is no clear analogue during creep deformation to a "work hardening" effect, there is a tendency for the stress and strain fields to become more "diffused" than during plastic deformation, such that pile-up (or "sink-in") effects are likely to be small.

5. Conclusions

The following conclusions can be drawn from this work:

(a) A procedure is described for iterative FEM simulation of the creep deformation that takes place during penetration of a spherical indenter into a sample (under constant applied load). The target outcome is a penetration-time dataset and convergence is obtained via optimisation of the set of 3 parameter values in the Miller-Norton creep law (covering both primary and secondary regimes).
(b) An important part of the procedure is the prior production on the sample surface of a recess that matches the (spherical) shape of the indenter. This ensures that the stresses in the sample can be kept below the yield stress throughout the indentation test, so that conventional plasticity (and the associated complications) can be avoided.
(c) Experimental work has involved a single material (pure Ni) at a single temperature (750°C). Both conventional uniaxial (tensile) creep tests, using three values for the applied (nominal) stress, and creep indentation testing, under a constant applied load, have been carried out. It is recognized that this constitutes a fairly limited dataset and the results presented are intended mainly to demonstrate the methodology and to obtain some preliminary indications regarding its reliability. Good agreement is observed between the strain-time plots obtained by conventional testing and by using the (Miller-Norton) creep parameter values inferred via the indentation testing. The stress exponent obtained in this way has a value of about 2.5.
(d) A final "tertiary" regime was observed with the higher stress level tensile tests, which was not captured well in the indentation-derived Miller-Norton curves. It seems likely that this arose because the true stress was approaching the yield stress, such that conditions were outside the regime that could be represented at lower stress levels by a Miller-Norton law with a single set of parameter values. Indeed, it may be that some conventional plastic deformation was starting to take place in the "tertiary" regime.
(e) Indentation creep plastometry does, of course, require a software package in order to infer strain-time curves from experimental indentation data. Such packages are now starting to become available for indentation plastometry and are likely to be developed soon for indentation creep plastometry - for example, see https://www.plastometrex.com/.

Declaration of Competing Interest

X The authors declare that they have no known competing financial interests or personal relationships that could have appeared to influence the work reported in this paper.

CRediT authorship contribution statement

M. Burley: Data curation, Investigation, Methodology, Writing - original draft. **J.E. Campbell:** Conceptualization, Writing - review & editing. **J. Dean:** Project administration, Writing - review & editing. **T.W. Clyne:** Conceptualization, Funding acquisition, Project administration, Supervision, Validation, Writing - review & editing.

Acknowledgements

This work has been supported by EPSRC (grant RG62695) and is part of an extended programme in the Gordon Laboratory aimed at development of indentation-based testing methodologies for obtaining bulk mechanical properties. There is extensive collaboration with a number of industrial partners in this work and the authors are grateful to Giles Aldrich-Smith and Nigel Park (both AWE), Richard Green (Solar Turbines), Jon Douglas (Frazer-Nash), Shiladitya Paul (TWI) and David Eaves (Westinghouse). Funding has also been received from the Leverhulme Trust (ref IN-2016-004), via a grant supporting the Leverhulme International Network on Composites for Extreme Temperatures (LINCET) . Activities in this Network include strong links with the group of Prof. Robert Vassen, in Forschungszentrum Jülich, with which collaborative research in this area is ongoing.

References

[1] Liu H, Chen Y, Tang Y, Wei S, Nuiu G. Tensile and indentation creep behaviour of mg-5%sn and mg-5%sn-2%di alloys. Mater Sci Eng A 2007;464:124–8.
[2] Takagi H, Dao M, Fujiwara M. Analysis on pseudo-steady indentation creep. Acta Mechanica Solida Sinica 2008;21:283–8.
[3] Marques VMF, Wunderle B, Johnston C, Grant PS. Nanomechanical characterisation of Sn-Ag-Cu/Cu joints - part 2: nanoindentation creep and its relationship with uniaxial creep as a function of temperature. Acta Mater 2013;61(7):2471–80.
[4] Geranmayeh AR, Mahmudi R. Indentation creep of a cast Mg-6Al-1Zn-0.7Si alloy. Mater Sci Eng A 2014;614:311–18.
[5] Chatterjee A, Srivastava M, Sharma G, Chakravartty JK. Investigations on plastic flow and creep behaviour in nano and ultrafine grain Ni by nanoindentation. Mater Lett 2014;130:29–31.
[6] Wang Y, Zeng J. Effects of Mn addition on the microstructure and indentation creep behaviour of the hot dip Zn coating. Mater Des 2015;69:64–9.
[7] Mahmudi R, Shalbafi M, Karami M, Geranmayeh AR. Effect of Li content on the indentation creep characteristics of cast Mg-Li-Zn alloys. Mater Des 2015;75:184–90.
[8] Ma Y, Peng GJ, Wen DH, Zhang TH. Nanoindentation creep behavior in a Cocrfecuni high-entropy alloy film with two different structure states. Mater Sci Eng A 2015;621:111–17.
[9] Ginder RS, Nix WD, Pharr GM. A simple model for indentation creep. J Mech Phys Solids 2018;112:552–62.
[10] Goodall R, Clyne TW. A critical appraisal of the extraction of creep parameters from nanoindentation data obtained at room temperature. Acta Mater 2006;54(20):5489–99.
[11] Chen J, Bull SJ. The investigation of creep of electroplated Sn and Ni-Sn coating on copper at room temperature by nanoindentation. Surf Coat Techn 2009;203(12):1609–17.
[12] Dean J, Campbell J, Aldrich-Smith G, Clyne TW. A critical assessment of the "Stable indenter velocity" method for obtaining the creep stress exponent from indentation data. Acta Mater 2014;80:56–66.
[13] Campbell J, Dean J, Clyne TW. Limit case analysis of the "Stable indenter velocity" method for obtaining creep stress exponents from constant load indentation tests. Mech Time-depend Mater 2016;1:31–43.
[14] Heinrich C, Waas AM, Wineman AS. Determination of material properties using nanoindentation and multiple indenter tips. Int J Solids Struct 2009;46:364–76.
[15] Dean J, Wheeler JM, Clyne TW. Use of Quasi-static nanoindentation data to obtain stress–strain characteristics for metallic materials. Acta Mater 2010;58:3613–23.
[16] Patel DK, Kalidindi SR. Correlation of spherical nanoindentation stress–strain curves to simple compression stress-strain curves for elastic-plastic isotropic materials using finite element models. Acta Mater 2016;112:295–302.
[17] Dean J, Clyne TW. Extraction of plasticity parameters from a single test using a spherical indenter and FEM modelling. Mech Mater 2017;105:112–22.
[18] Campbell JE, Thompson RP, Dean J, Clyne TW. Experimental and computational issues for automated extraction of plasticity parameters from spherical indentation. Mech Mater 2018;124:118–31.
[19] Campbell JE, Kalfhaus T, Vassen R, Thompson RP, Dean J, Clyne TW. Mechanical properties of sprayed overlayers on superalloy substrates, obtained via indentation testing. Acta Mater 2018;154:237–45.
[20] Meng L, Breitkopf P, Raghavan B, Mauvoisin G, Bartier O, Hernot X. On the study of mystical materials identified by indentation on power law and voce hardening solids. Int J Mater Form 2018.
[21] Campbell JE, Thompson RP, Dean J, Clyne TW. Comparison between stress–strain plots obtained from indentation plastometry, based on residual indent profiles, and from uniaxial testing. Acta Mater 2019;168:87–99.
[22] Liu YJ, Zhao B, Xu BX, Yue ZF. Experimental and numerical study of the method to determine the creep parameters from the indentation creep testing. Mater Sci Eng A 2007;456(1–2):103–8.
[23] Galli M, Oyen ML. Spherical indentation of a finite poroelastic coating. Appl Phys Lett 2008;93(3).
[24] Wu JL, Pan Y, Pi JH. On indentation creep of two Cu-based bulk metallic glasses via nanoindentation. Phys B-Condens Matter 2013;421:57–62.

[25] Dean J, Bradbury A, Aldrich-Smith G, Clyne TW. A procedure for extracting primary and secondary creep parameters from nanoindentation data. Mech Mater 2013;65:124–34.
[26] Su CJ, Herbert EG, Sohn S, LaManna JA, Oliver WC, Pharr GM. Measurement of power-law creep parameters by instrumented indentation methods. J Mech Phys Solids 2013;61(2):517–36.
[27] Cordova ME, Shen YL. Indentation versus uniaxial power-law creep: a numerical assessment. J Mater Sci 2015;50(3):1394–400.
[28] Rickhey F, Lee JH, Lee H. An efficient way of extracting creep properties from short--time spherical indentation tests. J Mater Res 2015;30(22):3542–52.
[29] Masayoshi S. Method for evaluation of creep characteristics. Pat. Appln. No. JP20100031502 2011.
[30] Tatsuya M. Measurement apparatus, test method, and physical property evaluation program for indentation creep test. Pat. Appln 2018 No. US201615577602.
[31] Dean J, Campbell JE, Burley M, Clyne TW. Indentation creep plastometry. Pat. Appln 2019 No. 1908656.0.
[32] Nelder JA, Mead R. A simplex method for function minimization. Comput J 1965;7(4):308–13.
[33] Gao FC, Han LX. Implementing the Nelder–Mead simplex algorithm with adaptive parameters. Comput Optim Appl 2012;51(1):259–77.
[34] Oliphant TE. Python for scientific computing. Comput Sci Eng 2007;9(3):10–20.
[35] van der Walt S, Colbert SC, Varoquaux G. The Numpy array: a structure for efficient numerical computation. Comput Sci Eng 2011;13(2):22–30.